

What molecules are able to treat *Madurella mycetomatis* eumycetoma *in vivo*?¹

Department of Pharmaceutical & Biological Chemistry, UCL School of Pharmacy

Abstract

Eumycetoma is a chronic inflammatory disease typically caused by *Madurella mycetomatis* fungal infection of the subcutaneous tissue with a characteristic discharge of dark grains. Current treatment of eumycetoma with antifungals of high *in vitro* potency has been disappointing with low cure rates of 25–35%. This has been attributed to the organisation of fungi within grain structures and the production of melanin as part of fungi adaptations to evade antifungal therapy. Hence, this study investigated the structure of *Madurella mycetomatis* grains and the effects of physiochemical properties (lipophilicity, molecular size and melanin binding capacity) of compounds on grain penetration. Through a literature synthesis, a model depicting the morphology and composition of *Madurella mycetomatis* grain was constructed. Densely-packed microcolonies of *Madurella mycetomatis* were identified to be embedded in a cross-linked cement-like grain matrix, surrounded by a triple-layered granuloma and an external collagen capsule. Previous research has noted that less lipophilic screening hits appeared to perform better in *in vivo* assays, independent of their *in vitro* potency. In this study, a statistically significant, negative correlation between LogD of those screening hits at pH 7.4 and percentage survival of *Madurella mycetomatis*-infected *Galleria mellonella* larvae was identified (Pearson's correlation, $r = -0.722$, $p = 0.002$, $n = 14$). This led to the proposal that four potential eumycetoma candidate compounds with $\text{LogD} \leq 2.0$ at pH 7.4 of promising *in vivo* efficacy, be prioritised for synthesis to enable antifungal susceptibility assays to be performed. No correlation between molecular weight or volume of compounds and their *in vivo* efficacy were identified in this study. Dichlorobenzene ring, extended polyaromatic side chain and positively-charged structures were among the identified moieties facilitating melanin binding which should be avoided in the design of future drug candidates. As the issue of grain penetration remains under-addressed, this study proposed a fluorescence assay using 8-amino BODIPY fluorophore which could be used to determine the accessibility of *Madurella mycetomatis* grains as part of future drug discovery projects.

¹ This is a data-mining project with a word count of 5996 words formatted in the printed style of PLOS Neglected Tropical Disease journal.

Introduction

Eumycetoma is a neglected tropical disease (NTD), endemic in tropical and subtropical countries [1]. It is a chronic, granulomatous, inflammatory disease of the subcutaneous tissue caused by a fungal infection [1]. The major causative fungus globally is *Madurella mycetomatis*, which is mainly found in animal dung and manure-enriched soil [2, 3]. Upon entry of *Madurella mycetomatis* into the subcutaneous tissue, a pathognomonic triad of subcutaneous nodules, multiple draining sinuses releasing pus, blood, serum and granular discharge containing pigmented hard grains are often the clinical presentation of most cases [1].

The typical eumycetoma intervention is a combination of surgery and extensive antifungal therapy with an average duration of 1.5 years [1, 4]. Surgery often involved amputations or excisions of infected lesions, resulting in permanent disability and functional loss of excised tissue [1]. To date, antifungals which have been used clinically in the treatment of eumycetoma include the azoles (posaconazole, itraconazole, ketoconazole, voriconazole), 5-flucytosine, caspofungin, terbinafine and amphotericin B [5]. Other drugs such as isavuconazole, ravuconazole, micafungin and anidulafungin have been tested in *in vitro* susceptibility assays but have not been used clinically [5]. Fosravuconazole, currently in Phase II/III trial is the first and only trial for investigating new treatment options for eumycetoma, which highlights its status as an NTD [6].

Based on the *in vitro* susceptibility of compounds determined by their MIC₉₀ values², *Madurella mycetomatis* is highly susceptible to the following azoles- posaconazole, itraconazole, ketoconazole, voriconazole, followed by amphotericin B, terbinafine and is resistant to 5-flucytosine and echinocandins [1]. However, *in vitro* susceptibility of *M. mycetomatis* hyphae does not correlate well to *in vivo* efficacy in animal models due to the aggregation of fungi within grain structures in *in vivo* settings [7]. In a murine model, grain formation was prevented in *M. mycetomatis* genome strain Mm55-infected mice treated with amphotericin B but not those treated with itraconazole, despite the latter having a 33-fold higher MIC₉₀ value² [1, 8].

A larval model was recently successfully developed as an alternative to mice due to structural and functional similarities in its innate immune system enabling the induction of grain formation *in vivo* [9, 10]. In this model, larvae of the *Galleria mellonella* wax moth infected with *Madurella mycetomatis* were able to produce

² MIC₉₀ values of antifungals tested against *Madurella mycetomatis*: Posaconazole (0.06 µM), itraconazole (0.06 µM), ketoconazole (0.125 µM), voriconazole (0.125 µM), amphotericin B (2 µM), terbinafine (8 µM), 5-flucytosine (>128 µM) and echinocandins (≥128 µM) [1].

histologically-similar grain structures, resembling those formed in the eumycetoma murine model and in humans [9]. *In vivo* assay results from this larval grain model were consistent with those in the murine model whereby only amphotericin B and terbinafine were able to prolong the survival of *M. mycetomatis* genome strain Mm55-infected larvae despite the azoles (ketoconazole, itraconazole, voriconazole and posaconazole) possessing much lower MIC₉₀ values² [1, 11].

It has been identified that *Madurella mycetomatis* is capable of producing melanin *in vivo* and *in vitro* via the 1,8-dihydroxynaphthalene (DHN)- and pyo-pathways, with only the former pathway contributing to reduced *in vitro* antifungal susceptibility [12, 13]. *M. mycetomatis* DHN-melanin conferred protection against itraconazole and ketoconazole as identified by elevations in MIC values of 16-fold and 32-fold, respectively in *in vitro* susceptibility assays [12]. This has been attributed to their ability in binding to DHN-melanin, preventing their access to their target, CYP450 14 α -demethylase [12].

Furthermore, the *in vitro* and *in vivo* susceptibilities of antifungals do not translate well to clinical outcomes as determined by the low cure rates of only 25-35% when patients were treated with susceptible antifungals monotherapy in clinical settings [6]. Dual combination therapies of three antifungals (amphotericin B, itraconazole or terbinafine) of different drug classes targeting ergosterol synthesis have been studied for *in vivo* efficacy in the larval grain model [14]. No evidence of synergistic effect in terms of prolongation of larval survival was noted [14]. Instead, lower overall survival rates were observed as compared to amphotericin B monotherapy [14]. This was attributed to the increased production of melanin and cement-like matrix formation in grains upon exposure of fungi to itraconazole and terbinafine [14]. Elevated melanin production, in turn, led to an increased binding to itraconazole and amphotericin B, inhibiting their access to drug targets, resulting in an undesired antagonistic effect of antifungal combination therapy [14].

In the recent screening of chemical libraries, several hit compounds such as 2-aminothiazole and fenarimol analogues with promising *in vivo* efficacy were identified and are currently being explored in the *Open Source Mycetoma* drug discovery project ([Fig 1](#)) [15, 16]. Analysis of the screening hits has led to the identification that compounds with lower values of LogD at physiological pH, representing lipophilicity, appeared to show higher *in vivo* efficacy as defined by their prolongation of *Madurella mycetomatis*-infected *Galleria mellonella* larval survival [15].

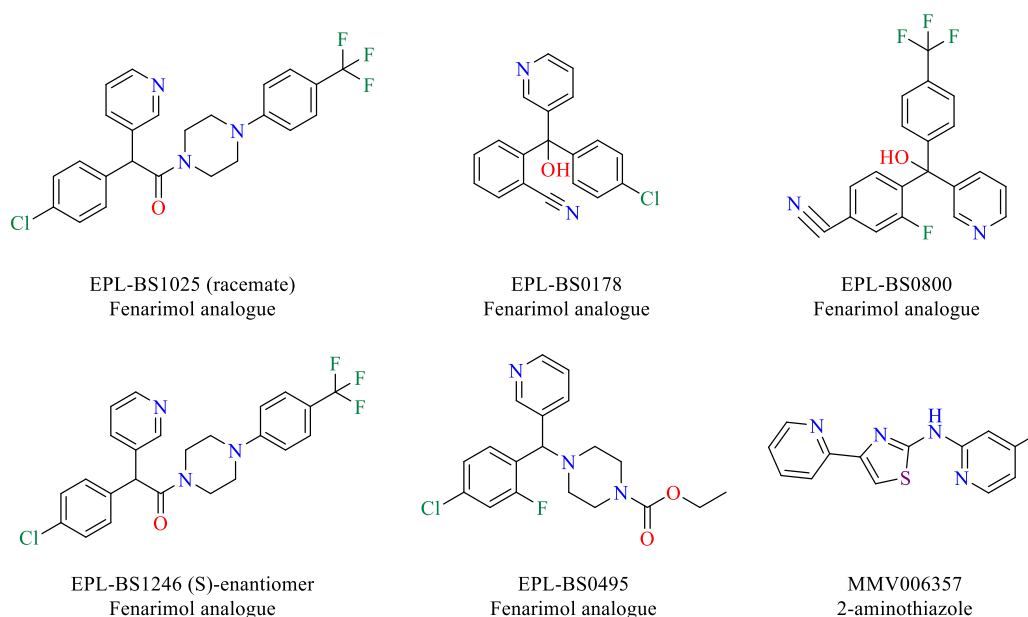


Fig 1. Graphical representation of 2-aminothiazole and fenarimol analogues identified in the screening of chemical libraries. The chemical structures of other identified hit compounds from the screening of Pathogen and Stasis Boxes are included in [S1 Appendix](#).

Overall, treatment has largely been extensive and ineffective with the added difficulty in discovering novel candidate compounds in that there is no correlation between *in vitro* potency and *in vivo* efficacy. The ability of *Madurella mycetomatis* to produce melanin and aggregate within grains in *in vivo* settings appear to be the key challenges in achieving a curative aim. Hence, this study was designed to investigate the following:

- Morphology and composition of *Madurella mycetomatis* grains.
- Physiochemical properties (lipophilicity, molecular size and melanin binding capacity) of small molecules and their effects on grain penetration.

Understanding these areas would aid the identification and optimisation of novel drug candidates. As the issue of grain penetration by compounds remains experimentally under-addressed, this study additionally proposes an assay using blue-emitting 8-amino BODIPY fluorophore that could be used in the qualitative and quantitative assessment of grain penetration.

Methods

A literature search³ using PubMed and Web of Science databases was undertaken to identify relevant literature on *Madurella mycetomatis* hard grains. Upon determination of grain morphology and composition, a model depicting the grain structure was constructed using Microsoft PowerPoint. As characteristic hard grains were additionally identified in *Streptomyces somaliensis* actinomycetoma bacterial infection, further literature search⁴ using the same databases was undertaken for the comparison of grain structures with those of *Madurella mycetomatis*.

To identify the effects of compound lipophilicity on *in vivo* efficacy, StarDrop-generated LogD at pH 7.4 and percentage survival of *Madurella mycetomatis*-infected *Galleria mellonella* larvae following treatment with clinically used antifungals and compounds identified from the screening of fenarimol library, Pathogen and Stasis Boxes were obtained from Dr. Wendy van de Sande of Erasmus Medical Centre, Dr. Benjamin Perry of Drugs for Neglected Diseases initiative (DNDi) and the Open Source Mycetoma GitHub platform (<https://github.com/OpenSourceMycetoma>). To identify the effects of molecular size and melanin binding capacity on *in vivo* efficacy, for all identified compounds tested in the larval grain model, their chemical structure and molecular weight were generated using ChemDraw Professional version 19.0.0.22 whereas their molecular volume was calculated using Molinspiration Cheminformatics version 2018.10.

From acquired data, scatterplots of larval survival against lipophilicity, molecular weight and molecular volume of compounds were constructed using Microsoft Excel. IBM SPSS Statistics version 26 was used to test for bivariate data normality using the Shapiro-Wilk test and to compute Pearson's product-moment correlation for statistical analysis of the correlation between lipophilicity and *in vivo* efficacy of compounds.

For the design of a fluorescence assay to determine grain penetration of compounds, a literature search⁵ using similar aforementioned databases was undertaken.

³ Search keywords: *eumycetoma*, *madurella-mycetomatis*, *eumycotic mycetoma*, *madura foot*.

⁴ Search keywords: *actinomycetoma*, *streptomyces-somaliensis*.

⁵ Search keywords: *blue-emitting fluorophore*, *fluorescence probe*, *fluorescence imaging*.

Results and Discussion

Grain morphology and composition

Madurella mycetomatis eumycetoma shows a unique clinical presentation with the discharge of dark-brown or black grains of 0.5-3.0 mm diameter observed from biological samples [17]. Although studies on the morphology and histochemistry of these grains have been conducted, rarely has a collation of the knowledge been documented or even interpreted graphically. As these studies often do not determine the genome of the specific strain of *M. mycetomatis* investigated, it cannot be confirmed if every known strain of *M. mycetomatis* displays the same morphology and composition as discussed below and depicted in [Fig 2](#) due to differences in genetic backgrounds.

Based on ultrastructural imaging and histochemical studies, *Madurella mycetomatis* was identified to organise into grain structures, with each grain within a granuloma surrounded by an external collagen capsule ([Fig 2](#)) [18]. These grains were only found *in vivo*, illustrating its role as a defence morphological adaptation of the fungi with protective roles against the host immune system and antifungal therapy [11].

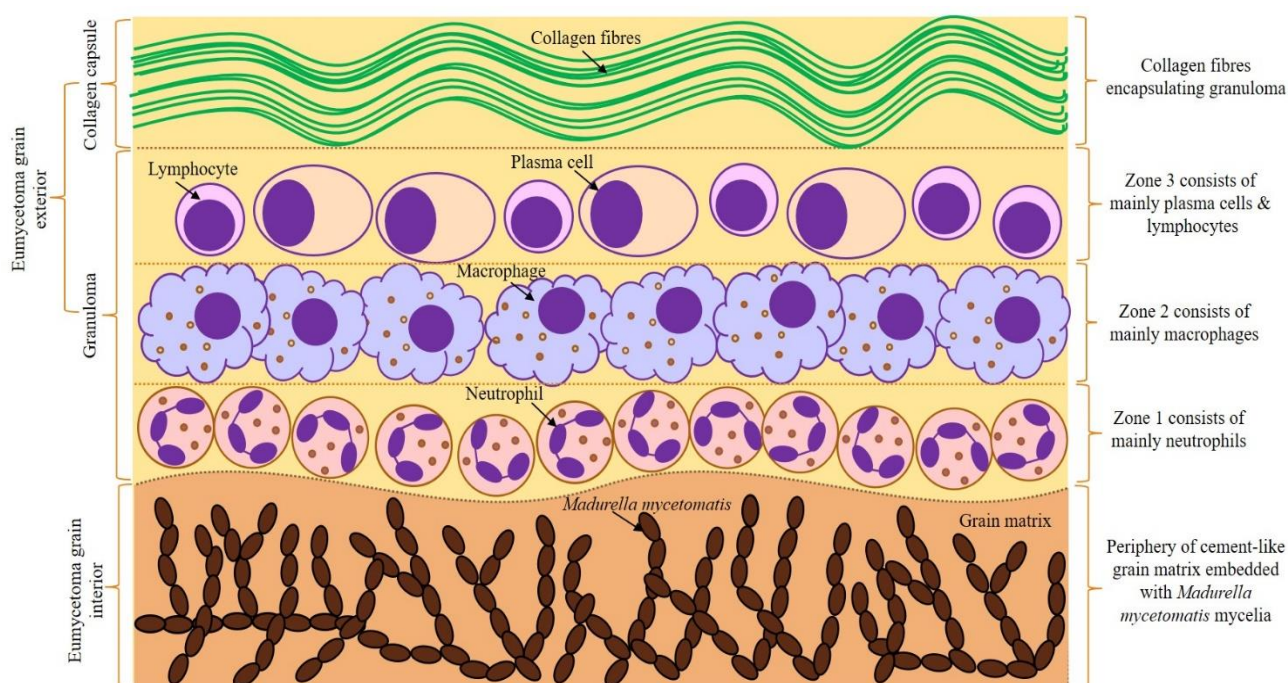


Fig 2. Conceptualisation of the layers surrounding *Madurella mycetomatis* *in vivo* and their known major constituents. Grain interior consists of *M. mycetomatis* embedded in a cement-like matrix whereas grain exterior consists of a granuloma and a collagen capsule. This diagram is meant for illustration purposes only and has not been constructed to the actual size, ratio, shape and colour of the major constituents present. An enlarged version of this diagram is included in [S2 Appendix](#).

Encapsulating the granuloma is a fibrous capsule of dense, thick collagen fibres as identified by Masson's trichrome and Sirius red stains [9, 18]. Surrounding the grain is a granuloma of a triple-layered zone of tissue reaction containing inflammatory and immune cells as part of the host immune response to pathogens [17]. The innermost layer (Zone 1) comprises of mainly neutrophils whereas the middle layer (Zone 2) consists of mainly macrophages with melanin pigment within their cytoplasm, indicative of their phagocytosis execution ability [17]. The outer layer (Zone 3) consists of mainly plasma cells, lymphocytes and multinucleated giant cells [17]. The granuloma also comprises of diffusely scattered melanin-pigmented histiocytes and haemosiderin from extravasated erythrocytes, identified by Masson-Fontana and Prussian blue stains, respectively [19]. Within the granuloma, matrix metalloproteinases (MMP-2, MMP-9), cytokines (IL-17A, IL-10) and chemokine CCL-5, produced by neutrophils, macrophages and lymphocytes were also identified from several studies [18, 20, 21].

Embedded within grain matrices are intercalating *Madurella mycetomatis* mycelia with branched, septated and radially-arranged hyphae of 2-5 μm diameter [22, 23]. Ultrastructural images revealed that hyphae were either vesicular or filamentous with multiple, 0.2-2.0 μm thickened and occasionally concentric layers in cell walls due to intra-hyphal hyphae growth [23]. From histochemical studies, hyphal cell walls were found to contain chitin, chitin-bound chitinases such as host-derived chitotriosidase and acidic mammalian chitinase, β -1,3-glucan polysaccharide, melanin and fine bundles of collagen [24-26].

Within the grains, microcolonies of densely-packed *Madurella mycetomatis* mycelia are embedded in a resilient cement-like matrix [7]. This cross-linked matrix was found to contain proteins, lipids, melanin at grain periphery and heavy metals such as copper, zinc and calcium [12, 16, 26]. To date, there are no known studies determining the exact nature, components and ratio of the proteins and lipids in the grain matrix but its cross-linked structure likely impedes the ease of accessibility of antifungals to embedded fungi.

Melanisation was identified to be essential in cement-like matrix formation as melanin is capable of binding to other components such as collagen fibres, forming a complex which makes up the grain matrix [27]. This binding capacity of melanin also explains their localisation at grain periphery and in cell walls of embedded hyphae. Based on *in vitro* studies of *M. mycetomatis* incubated with melanin synthesis inhibitors, it was determined that *M. mycetomatis* is capable of synthesising pyomelanin and DHN-melanin [12]. To date, the complete

structure and aromatic-aliphatic ratio of *M. mycetomatis* melanin have not been elucidated, owing to its complex amorphous structure and insolubility in organic and inorganic solvents making it harder to study using traditional crystallography methods [26, 28, 29].

As compared to normal subcutaneous tissue, elevated amounts of host-derived zinc (6-fold), copper (4-fold) and calcium (16-fold) ions bound to melanin within the grains were detected through atomic absorption spectrophotometry [26]. Previous studies have identified that the high binding capacity of fungi melanin relates to their functional groups, such as the presence of carboxyl groups facilitating binding to calcium and zinc, and hydroxyl groups enabling binding to copper [26, 30]. Elevation of copper may relate to their role as a co-factor in melanin biosynthetic pathways as they aid the enzyme-substrate alignment in melanin biosynthesis [30]. Copper also has a role in collagen fibre formation, which explains its deposition in the cell wall and external collagen capsule encapsulating the granuloma [19]. The role of zinc in *Madurella mycetomatis* has not been studied but previous research on other fungi have identified the existence of copper- and zinc-dependent superoxide dismutases which scavenge neutrophil-secreted reactive oxygen species [31]. This is consistent with experimental evidence that *M. mycetomatis* melanin, of which metal ions are bound to, was capable in scavenging permanganate, highlighting its protective ability against host-induced oxidative stress [12]. Calcium which was identified to be localised in hyphae cell walls, melanin sites within grain matrix and surrounding the grain interior, likely contributes to grain resilience [26]. Overall, identified metal ions appear to have roles in grain matrix formation and fungi defence mechanism against antifungals and the host immune system.

Comparison between hard grains of *Streptomyces somaliensis* and *Madurella mycetomatis*

Unlike eumycetoma with low cure rates of 25-35% with antifungal monotherapy, actinomycetoma shows a cure rate of around 90% with the current first-line combination therapy of co-trimoxazole and amikacin sulfate [1, 6, 32]. Since actinomycetoma is relatively susceptible to treatment in comparison to eumycetoma, further research into a common actinomycetoma-causative agent, *Streptomyces somaliensis*, known to form yellow-brown hard grains was conducted to compare the structure of the grains and their surrounding layers with those of *Madurella mycetomatis* [1, 17].

Based on the ultrastructural imaging and histochemical staining of biological samples infected with *Streptomyces somaliensis*, 0.2-0.8 mm grains were observed to contain septated bacterial filaments with thick cell walls embedded in a reticulate cement-like matrix which provides structural integrity to the grains [33]. From ultrastructural and immunohistochemistry studies, *Streptomyces somaliensis* grains were identified to be surrounded by a similar triple-layered zone of tissue reaction containing neutrophils, macrophages, lymphocytes, plasma cells and giant cells, as described [earlier](#) for *M. mycetomatis* grains [33, 34]. The cement-like matrix in *S. somaliensis* was found to consist of a meshwork of mucopolysaccharide fibrillar substances at grain periphery, secreted 15.5 kDa exotoxin and incorporated immune cells such as macrophages and giant cells [33, 35]. The penetration of neutrophils into the cement-like matrix likely facilitated the entry and incorporation of immune cells within the grain matrix [34, 35].

Several notable differences between the grains of *Streptomyces somaliensis* and *Madurella mycetomatis* were identified. In terms of grain size, *S. somaliensis* grains are much smaller than *M. mycetomatis* grains of 0.5-3.0 mm in diameter [17]. Secondly, within the grain matrix, unlike *M. mycetomatis* grains with densely-packed fungi aggregates, *S. somaliensis* grains possess multiple clear spaces free of bacterial filaments within the matrix [33]. Although neutrophils have been identified to infiltrate the grain matrices of both pathogens, macrophages and giant cells were incorporated as part of the cement-like matrix in only *S. somaliensis* grains [33]. Lastly, there is no evidence of melanin production by *S. somaliensis* unlike *M. mycetomatis*, but its resilient, cement-like matrix consisting of a meshwork structure shares some similarities with the cross-links in *M. mycetomatis* grain matrix [16, 33].

As the exact composition of both *Madurella mycetomatis* and *Streptomyces somaliensis* have not been fully elucidated, the evidence available for grain comparison is limited and it appears that the only similarities between both grains are the cross-linked meshwork structure of grain matrix, grain hardness and integrity. Although several differences were noted earlier, of particular relevance in this study is the lack of melanin production in *S. somaliensis*, which may in part explain the difference in clinical cure rates due to the melanin barrier preventing the access of antifungals to grain-embedded fungi.

Analysis of physiochemical properties of amikacin sulfate and cotrimoxazole, the current first-line treatment options of actinomycetoma, revealed that both drugs possess high molecular weight (>500 Da) and low lipophilicity as determined by their StarDrop-generated LogD at pH 7.4 of -1.6 and 0.5,

respectively (Fig 3) [36]. Despite being large molecules, their low lipophilicity appears to facilitate their penetration into *S. somaliensis* grains.

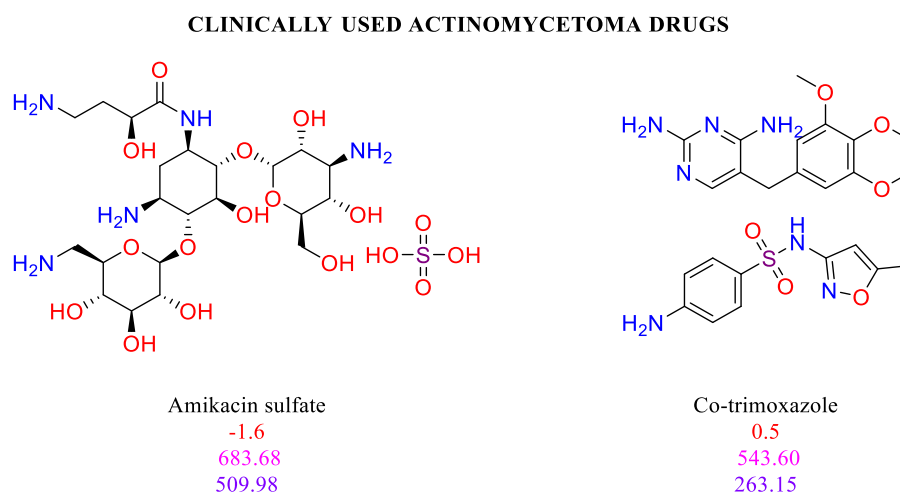


Fig 3. Graphical representation of actinomycetoma first-line treatment options: Amikacin sulfate and co-trimoxazole. The LogD at pH 7.4, molecular weight (Da) and molecular volume (\AA^3) of drugs are depicted in red, pink and purple, respectively.

Effects of physiochemical properties of compounds on *in vivo* efficacy

Lipophilicity-correlated efficacy

As drugs of low lipophilicity were able to penetrate *Streptomyces somaliensis* grains, an analysis of lipophilicity of all compounds tested in the *in vivo* *Galleria mellonella* larval grain model which included 14 screening hits (Table 1) and an additional six antifungals used clinically in eumycetoma treatment (Table 2) was undertaken (S2 Appendix). Compound lipophilicity was defined by its LogD value at pH 7.4 generated using StarDrop software and *in vivo* efficacy was defined by the percentage survival of *Madurella mycetomatis*-infected *Galleria mellonella* larvae after 10 days following administration of either fixed 20 μ M concentration of compounds in Table 1 or varying human pharmacokinetic equivalent dosages of antifungals in Table 2 [11, 15]. The difference in overall percentage survival of larvae after 10 days reflects the varying ability of compounds to penetrate grain structures and their subsequent binding interactions with drug targets and grain matrix components such as melanin. As determined in previous studies and shown in Tables 1 and 2, only ten compounds were able to significantly enhance larval survival as compared to controls treated with either phosphate-buffered saline or 5% glucose (Log-Rank test, $p < 0.05$) [11, 15]. These ten compounds were deemed as

being capable of penetrating the grains to reach their targets as demonstrated by their *in vivo* efficacy in prolonging larval survival.

Table 1. Percentage survival of *Madurella mycetomatis*-infected *Galleria mellonella* larvae treated with 20 μ M of the following screening hit compounds and their respective StarDrop-generated LogD at pH 7.4, molecular weight and calculated molecular volume [15, 36].

Drug Class	Screening hit compound ID	Lipophilicity (StarDrop-generated LogD at pH 7.4)	Molecular weight (Da)	Calculated molecular volume (\AA^3)	<i>In vivo</i> efficacy (Percentage survival of <i>Galleria mellonella</i> larvae administered with 20 μ M of compound per larvae after 10 days) (%)
Fenarimol	EPL-BS0178	2.3	320.8	277.6	36.7*
	EPL-BS0495	2.5	377.8	329.9	24.1*
	EPL-BS1025 (racemate of EPL-BS1246)	3.5	459.9	385.3	19.2*
	EPL-BS0800	3.1	372.3	300.3	10.0
	EPL-BS1246 (S-enantiomer)	3.5	459.9	385.3	7.1
Azole	MMV688774 (Posaconazole)	3.5	700.8	623.4	18.6*
	MMV688943 (Difenoconazole)	4.3	406.3	330.6	13.8
	MMV688942 (Bitertanol)	4.2	337.4	320.8	11.5*
Strobilurin	MMV688754 (Trifloxystrobin)	4.2	403.4	345.7	15.6
	MMV021057 (Azoxystrobin)	4.0	403.4	350.9	21.4
Pyrazolo-pyrimidine	MMV022478	3.1	432.9	374.4	18.5*
Benzamide	MMV687807	4.6	383.7	271.0	6.9
Quinazoline	MMV675968	2.0	359.8	307.5	23.3*
2-aminothiazole	MMV006357	2.2	268.3	234.1	28.6*

Significant survival displayed as * (Log-Rank test, $p < 0.05$) [15].

Table 2. Percentage survival of *Madurella mycetomatis*-infected *Galleria mellonella* larvae treated with varying concentrations of the following clinically used antifungals and their respective StarDrop-generated LogD at pH 7.4, molecular weight and calculated molecular volume [11, 36]. Human pharmacokinetic equivalent dosages of compounds administered were converted to their comparable micromolar concentrations.

Drug Class	Clinically used antifungal	Human pharmacokinetic equivalent dosage (mg/kg)	Calculated dosage given (μ M)	Lipophilicity (StarDrop-generated LogD at pH 7.4)	Molecular weight (Da)	Calculated molecular volume (\AA^3)	<i>In vivo</i> efficacy (Percentage survival of <i>Galleria mellonella</i> larvae after 10 days) (%)
Azole (Triazole)	Posaconazole	5.7	14.0	3.5	700.8	623.4	4.4
	Itraconazole		8.1	4.5	705.6	607.9	6.7
	Voriconazole		16.3	2.5	349.3	285.1	11.1
Azole (Imidazole)	Ketoconazole		10.7	3.0	531.4	452.5	6.7
Polyene	Amphotericin B	14.0	15.1	1.1	924.1	865.5	23.3*
Allylamine	Terbinafine	1.0	3.4	3.6	291.4	306.7	20.5*

Significant survival displayed as * (Log-Rank test, $p < 0.05$) [11].

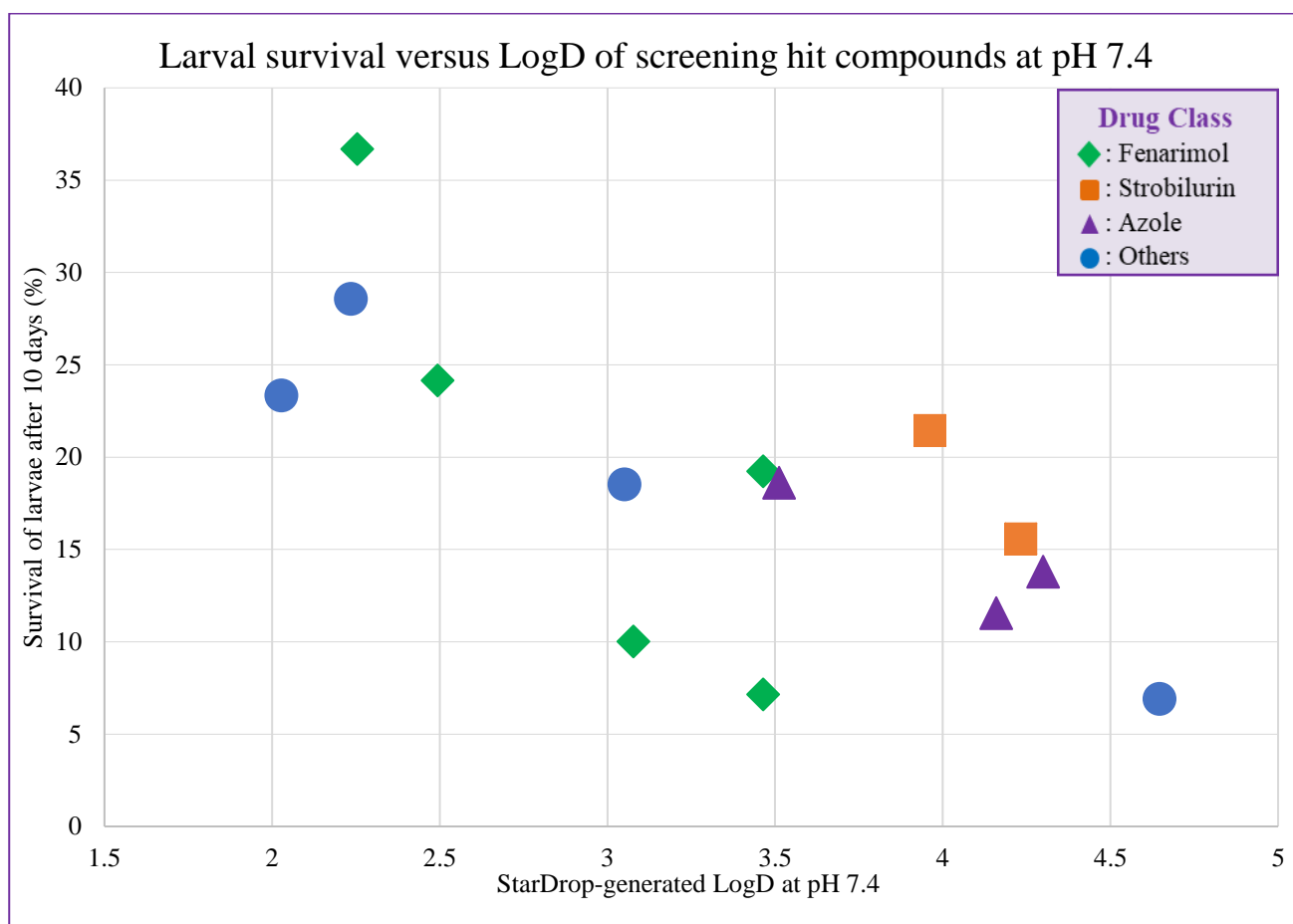


Fig 4. Graphical representation of the data shown in Table 1 with a negative correlation observed between percentage survival of larvae and LogD of screening hit compounds at pH 7.4. Percentage survival of *Galleria Mellonella* larvae infected with *M. mycetomatis* is displayed on the vertical axis and the StarDrop-generated LogD of administered compounds at pH 7.4 is displayed on the horizontal axis. The legend at the right corner depicts the known major drug classes of antifungals.

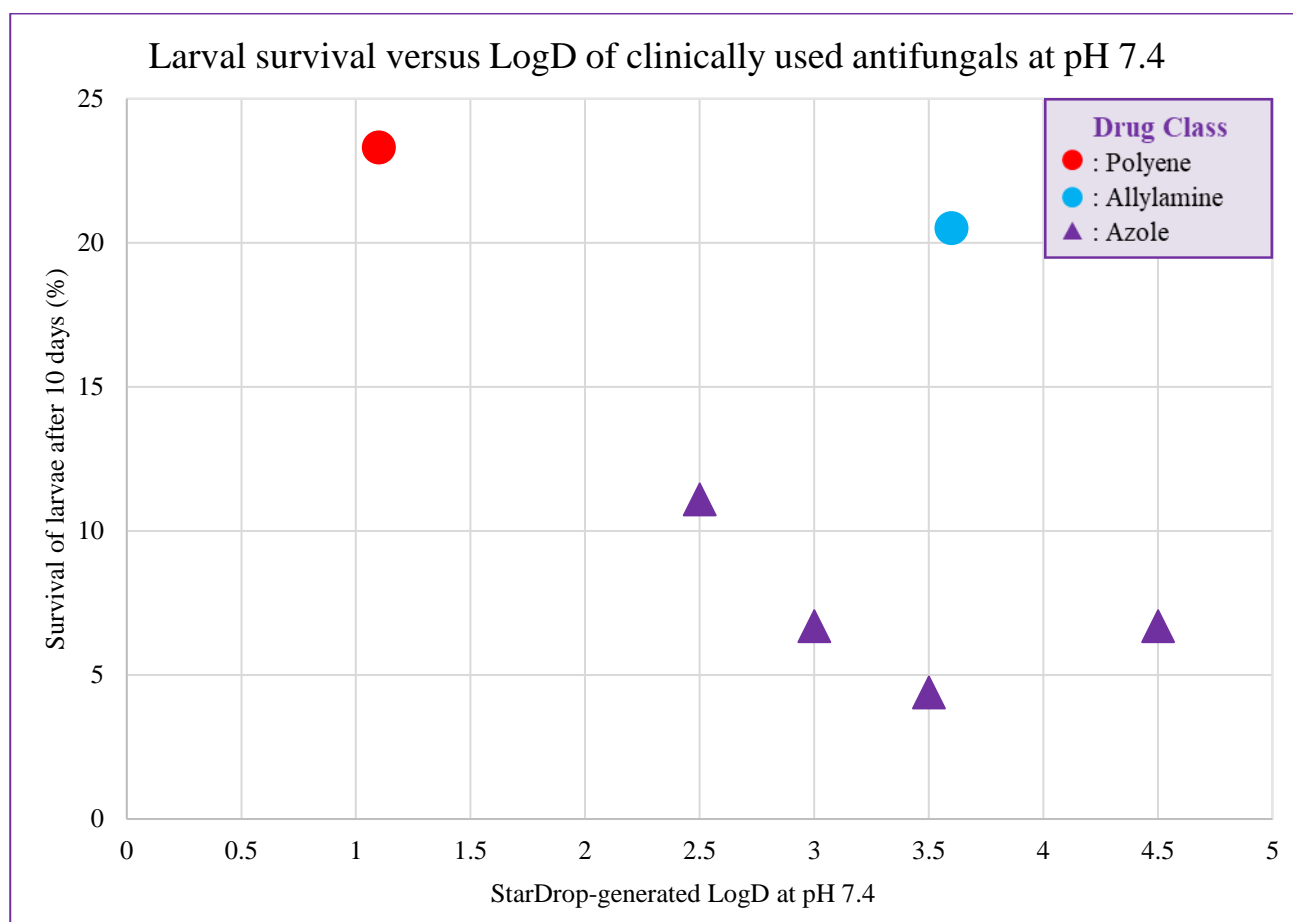


Fig 5. Graphical representation of the data shown in [Table 2](#) with a negative correlation observed between percentage survival of larvae and LogD of clinically used antifungals at pH 7.4. Percentage survival of *Galleria Mellonella* larvae infected with *M. mycetomatis* is displayed on the vertical axis and the StarDrop-generated LogD of administered compounds at pH 7.4 is displayed on the horizontal axis. The legend at the right corner depicts the major drug classes of antifungals.

Two scatterplots were constructed to visualise the spread and relationship of the data in [Tables 1](#) and [2](#) relating the percentage survival of *M. mycetomatis*-infected *Galleria Mellonella* larvae with the StarDrop-generated LogD of compounds at pH 7.4 when administered at various concentrations ([Figs 4](#) and [5](#)). From the visual inspection of the scatterplots, there is a general impression that reduced lipophilicity as determined by lower LogD at pH 7.4 value is associated with increased *in vivo* efficacy as defined by higher percentage survival of infected larvae following administration of compounds, regardless of their structural diversity ([S2 Appendix](#)). Despite being administered at lower concentrations, amphotericin B and terbinafine were able to significantly prolong larval survival with higher survival rates than the majority of compounds in [Table 1](#) (Log-Rank test, $p < 0.05$) [11].

Since a negative trend was observed in both scatterplots, the set of data variables (LogD of compounds at pH 7.4 and percentage survival of infected

larvae) in Tables 1 and 2 were first quantitatively assessed for a normal distribution using the Shapiro-Wilk test to determine the method of statistical analysis of correlation (S3 Appendix) [37]. As data normalities for both variables were identified, Pearson's product-moment correlation coefficient, r was computed to determine the strength and significance of the observed trends between lipophilicity and *in vivo* efficacy from the scatterplots.

Table 3. Pearson's product-moment correlation test results showing a negative correlation between lipophilicity of the following compounds and their *in vivo* efficacy.

	Table 1 compounds	Table 2 compounds	Fenarimol compounds in Table 1
Pearson's correlation coefficient, r	-0.722	-0.609	-0.818
Number of compounds, n	14	6	5
p value (one-tailed)	0.002*	0.1	0.045*

Significant p values displayed as * ($p < 0.05$).

As shown in Table 3, a strong⁶, statistically significant negative correlation between lipophilicity of Table 1 compounds and *in vivo* efficacy was identified ($r = -0.722$, $p = 0.002$, $n = 14$) whereas for Table 2 compounds, a moderate⁶, non-statistically significant negative correlation between both data variables was identified ($r = -0.609$, $p = 0.1$, $n = 6$) [38]. The statistical insignificance of the latter is likely due to the small sample size of only 6 compounds tested but it does not dismiss the identified negative correlation between data variables which is relevant in preclinical drug research.

In the series of fenarimol compounds, a strong⁶, statistically significant negative correlation between lipophilicity and *in vivo* efficacy with a larger r value was identified ($r = -0.818$, $p = 0.045$, $n = 5$). This indicates that comparing the StarDrop-generated LogD values across heterogeneous compounds with structural diversity is less reliable than comparing within a chemical series of homologous compounds [39]. However, the correlation coefficients for other chemical series were not computed due to the small sample size (≤ 2) of compounds within other series and the heterogeneity of variants within the azole series such as the imidazoles and triazoles (Table 2). Statistical analyses of the data do not, however, justify a causal relationship between compound lipophilicity and *in vivo* efficacy but merely an association between the two data variables. The identified negative correlations for all compounds indicate that the penetration of compounds into

⁶ Pearson's correlation coefficient was interpreted using a conventional stratification listed in S3 Appendix.

Madurella mycetomatis grains is enhanced when their lipophilicity is reduced, implying that the grain components shown in Fig 2 are likely overall less lipophilic as well.

Hence, low lipophilicity, defined as LogD values of ≤ 2.0 at pH 7.4 is proposed as the key criterion in the identification and design of novel drug candidates. Through a search in the list⁷ of compounds suggested by Drugs for Neglected Diseases *initiative* (DNDi) and members of the Open Source Mycetoma, seven compounds were identified to possess StarDrop-generated LogD values of ≤ 2.0 at pH 7.4, indicative of promising *in vivo* efficacy (Fig 6) [16]. Since a lipophilicity-correlated efficacy was identified, it is proposed that the four compounds shown within the green box in Fig 6 be prioritised for synthesis to enable antifungal susceptibility assays to be conducted to determine if they are effective drug candidates for *Madurella mycetomatis* eumycetoma.

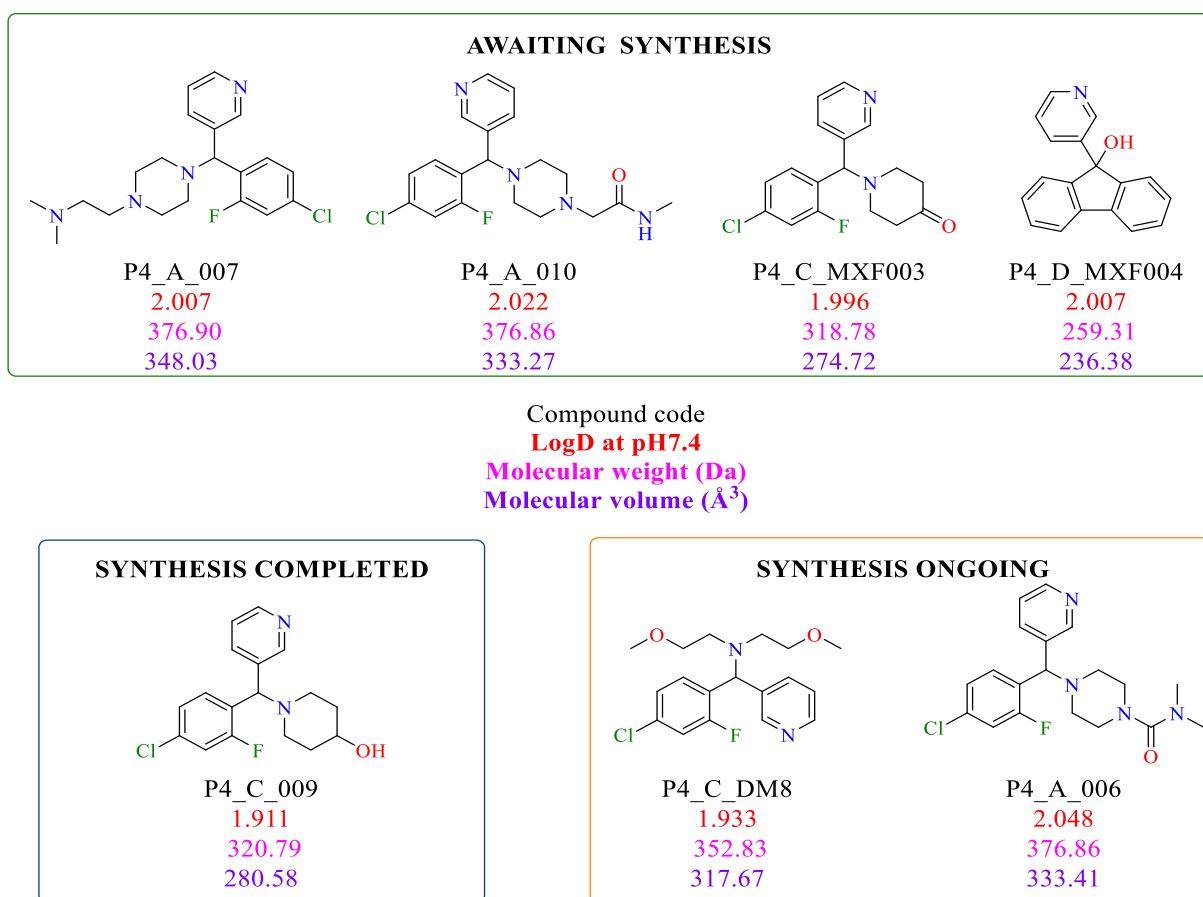


Fig 6. Graphical representation of potential drug candidates with LogD ≤ 2.0 at pH 7.4. The compound code, LogD at pH 7.4, molecular weight (Da) and molecular volume (Å³) are depicted in black, red, pink and purple, respectively. Compounds in the green box have yet to be synthesised whereas compounds in the orange box are currently being synthesised. The single compound in the blue box has been synthesised but it has not been tested in *in vitro* and *in vivo* susceptibility assays.

⁷ The Open Synthesis Network Master List consisting of 52 suggested compounds was accessed through the Open Source Mycetoma GitHub platform: https://github.com/OpenSourceMycetoma/Series-1-Fenarimols/blob/master/OSN_P4%20MycetOS%20lists.zip.

Molecular size considerations

The structure, size and porosity of melanin in *Madurella mycetomatis* hyphal walls have not been discerned down to the ultrastructural level [26]. However, cryoporometry studies of another fungus, *Cryptococcus neoformans* with similarly melanised concentric wall layers as *M. mycetomatis* have identified that melanin layers are porous, with a diameter of pores between melanin particles ranging between 1-4 nm and some up to 30 nm [12, 28]. However, as *C. neoformans* produces melanin by the pyo- and DOPA-pathways, with only the former pathway being similar to *M. mycetomatis*, it remains unknown if the identified pore diameter range differs between DHN-melanin and DOPA-melanin [12].

As evidence of elevated amounts of host-acquired calcium, zinc and copper were previously identified within *Madurella mycetomatis* cement-like grain matrix and uptake of nutrients such as glucose and amino acids occurs via the tips of fungi hyphae, these findings suggest that small molecules are capable of penetrating the grain and subsequently the embedded melanised hyphae [7, 26]. Since X-ray crystallography studies determining the three-dimensional geometry of compounds in Tables [1](#) and [2](#) have not been conducted, as approximate descriptors of molecular size, the molecular weight and volume of compounds were analysed to determine if the grain structure has a size exclusion barrier. Two scatterplots were constructed depicting the percentage survival of *Madurella mycetomatis*-infected *Galleria mellonella* larvae and the molecular weight and volume of administered compounds (Figs [7](#) and [8](#)).

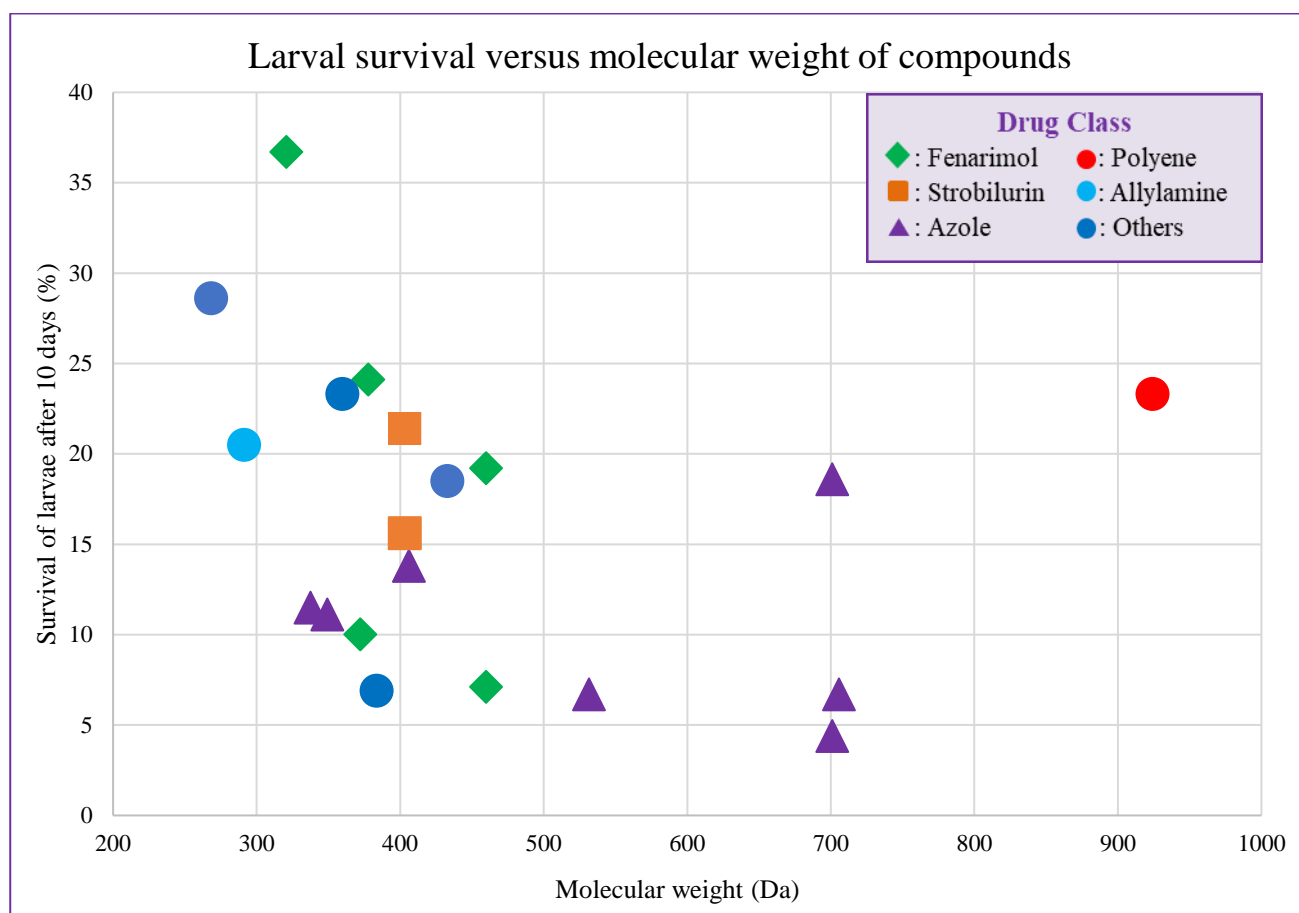


Fig 7. Graphical representation of the data shown in Tables 1 and 2 with no correlation observed between percentage survival of larvae and molecular weight of administered compounds. Percentage survival of *Galleria Mellonella* larvae infected with *Madurella mycetomatis* is displayed on the vertical axis and the molecular weight of compounds is displayed on the horizontal axis. The legend at the right corner depicts the known major drug classes of antifungals.

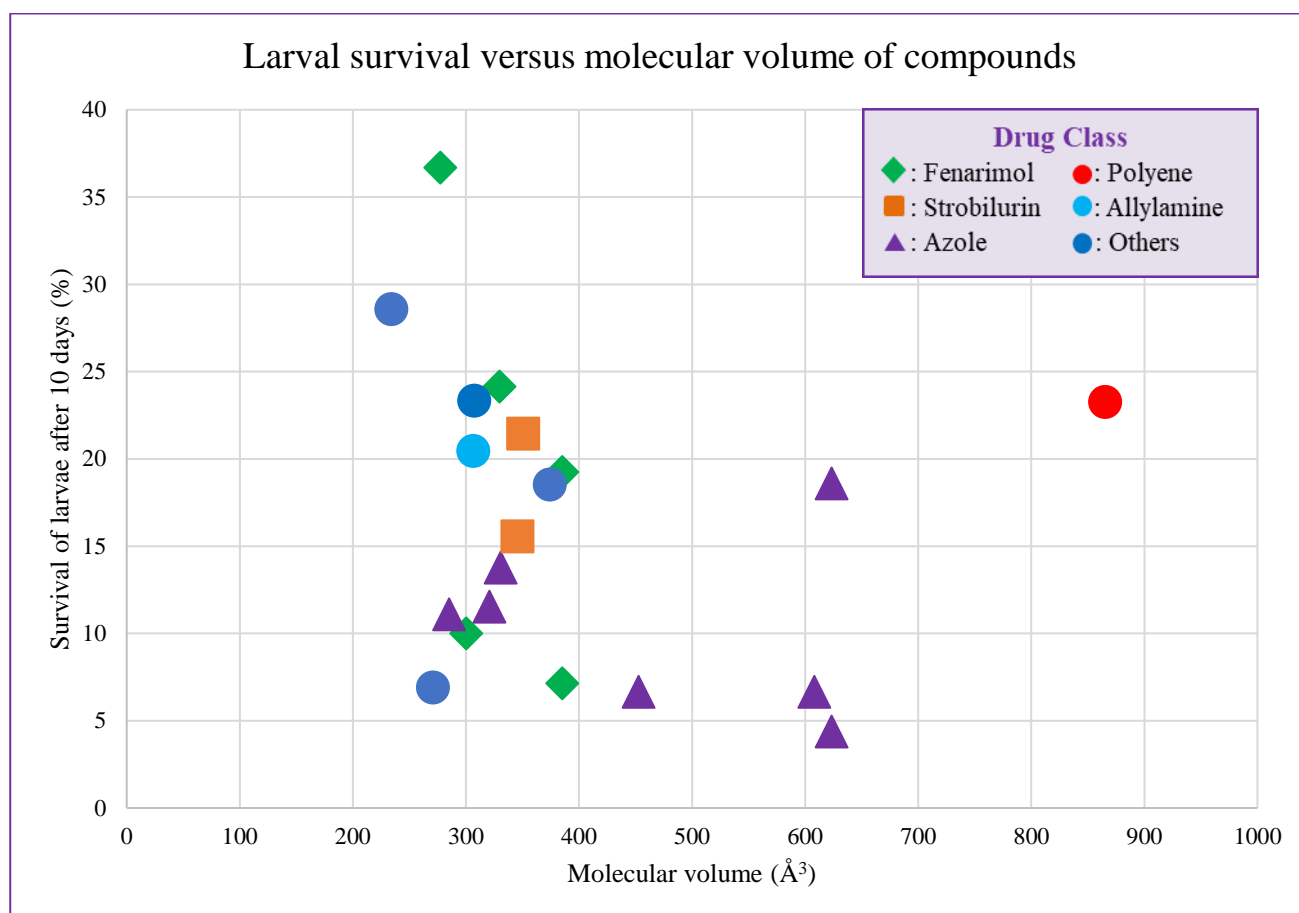


Fig 8. Graphical representation of the data shown in Tables 1 and 2 with no correlation observed between percentage survival of larvae and molecular volume of administered compounds. Percentage survival of *Galleria Mellonella* larvae infected with *Madurella mycetomatis* is displayed on the vertical axis and the molecular volume of compounds is displayed on the horizontal axis. The legend at the right corner depicts the known major drug classes of antifungals.

Although the molecular weight and volume of compounds studied cover a wide range (268-924 Da and 234-865 Å³), they were all clustered ≤500 Da and ≤400 Å³, with the exception of posaconazole, itraconazole, ketoconazole and amphotericin B. As both scatterplots did not show a correlation between molecular size of compounds and their *in vivo* efficacy, it appears that molecular size is not a dominating determinant of *in vivo* efficacy. However, it still remains unclear if *M. mycetomatis* grain structure has a size exclusion barrier, as using molecular weight and volume as approximate size descriptors do not account for the molecular shape of compounds which may additionally influence the diffusion of compounds through the cross-linked grain matrix and their subsequent accessibility to grain-embedded fungi [40]. Further research on the molecular shape of compounds using descriptors such as Molecular Shape Index to gauge the degree of compound linearity or sphericity could be conducted to determine its effect on grain penetration [41].

As no measurement of intragrain compound concentration and drug-target binding assays have been conducted for compounds in Tables 1 and 2, the use of larval survival data alone remains limited as an indirect approximate measure of grain penetration and subsequent drug target accessibility of compounds. Hence, the actual influence of lipophilicity and molecular size of compounds on grain penetration remain unknown.

Structures facilitating melanin binding

Madurella mycetomatis was identified to be capable of producing either DHN-melanin, pyomelanin, or both depending on its genome strain [12, 13]. A previous study comparing the MIC₉₀ values of azoles, echinocandins, amphotericin B and 5-flucytosine for *M. mycetomatis* isolates with and without pyomelanin secretion identified that pyomelanin did not influence the *in vitro* susceptibilities of *M. mycetomatis* isolates to antifungals [13]. In contrast, binding of DHN-melanin to itraconazole and ketoconazole has been associated with elevated MIC values of 16-fold and 32-fold, respectively [12]. However, there were no shifts in MIC values for voriconazole and fluconazole which did not bind to DHN-melanin [12]. Selective binding of DHN-melanin to certain azoles led to the identification of dichlorobenzene ring and extended polyaromatic side chain as the structures present only in itraconazole and ketoconazole which likely facilitated the binding interaction with melanin (Fig 9) [12].

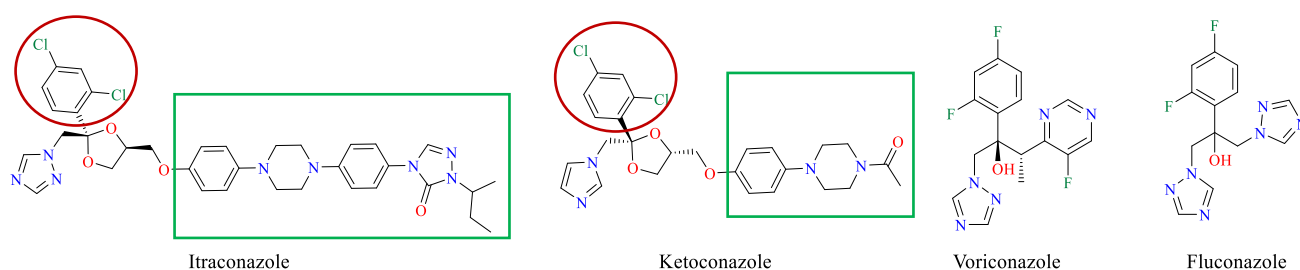


Fig 9. Identification of dichlorobenzene ring (red oval) and extended polyaromatic side chains (green box) in itraconazole and ketoconazole which facilitate binding with *Madurella mycetomatis* DHN-melanin. These identified structures were not present in voriconazole and fluconazole [12].

As melanin was identified to be a major component of the *Madurella mycetomatis* grain structure, with dense layers deposited in the concentric hyphal wall layers and diffused within the cement-like grain matrix, the binding potential of novel candidate compounds to DHN-melanin should ideally be minimal as this could prevent their accessibility and interaction with drug targets and subsequent effects on fungi growth or viability [12, 23, 26]. Although the exact chemical

structure of *M. mycetomatis* melanin remains unknown, it likely shares similar general physiochemical properties as the family of melanins produced by other fungi through the same pathways, of which polymerisation of phenolic precursors results in a polyanionic, aromatic and hydrophobic melanin macromolecule [29, 42]. This hypothesis can be supported by various notable similarities in the behaviour of *M. mycetomatis* melanin in terms of its antioxidant properties, its binding capacity to metal ions and to antifungals [12]. Previous studies have attributed the high binding capacity of fungi melanin to its carboxyl, phenol, hydroxyl and amine functional groups which facilitate the formation of ionic, covalent and hydrophobic interaction with compounds [30]. Therefore, although none of the identified screening hits and proposed compounds in [Fig 6](#) has the dichlorobenzene ring and extended polyaromatic side chains structures linked to melanin binding interaction, until drug-melanin binding assays have been conducted, it is not possible to dismiss the possibility that there may be other structures facilitating the binding interaction with *M. mycetomatis* melanin ([S1 Appendix](#)).

Although having charged groups at physiological pH would contribute to reduced lipophilicity, enhancing *in vivo* efficacy, as fungi melanin is known to be negatively-charged, opposing charges would promote their binding interaction with melanin [12]. Previous study has identified that phage with positive charges and aromatic residues were bound to *Cryptococcus neoformans* melanin, indicating that fungi melanin possesses these similar structures allowing binding interaction with the phage [43].

Overall, for compounds to reach their drug targets in grain-embedded fungi, the aforementioned structures facilitating melanin binding interaction should ideally be avoided in the design of future drug candidates.

Design of a fluorescence assay

As grain penetration is a prerequisite for the binding interaction of compounds with drug targets and their subsequent effects on fungi growth or viability, the design of a first-ever fluorescence assay to determine grain penetration by small molecules would be beneficial in future drug discovery projects. Through this assay, an analysis of the physiochemical characteristics of assayed compounds would provide information on the properties facilitating grain penetration. This could then be used as the selection criteria in the screening of chemical libraries to identify compounds capable of grain penetration and to

optimise the design of identified hits by chemical modification for enhanced grain penetrability [44].

In the design of the fluorescence assay, selection of a blue-emitting fluorophore would be ideal to differentiate fluorophore signals from background autofluorescence of the cement-like grain matrix, occurring in the red and green spectral regions [45]. While there are several blue-emitting fluorophores based on coumarin core structure such as Pacific Blue, Alexa Fluor 350 and aminomethylcoumarin acetate which are potential candidates, they experience rapid chemical photobleaching and are sensitive to environmental polarity changes, leading to quenching and shifts in emission wavelengths of fluorescence (Fig 10) [46, 47].

In an *in vitro* susceptibility assay, *Madurella mycetomatis* pyomelanin interfered with the reduction of resazurin fluorometric indicator to fluorescent resorufin, likely through the formation of a pyomelanin-resazurin complex which inhibited its reduction to resorufin [13]. Hence, apart from pyomelanin, the ability of other grain constituents to interfere with fluorescence emission and their influence on the overall polarity of intragrain environment, which remain unknown, are critical considerations in the assay design. Therefore, in the proposed assay (Protocols A and B), 8-amino BODIPY was selected as an alternative to coumarin-based fluorophores owing to its photostability, environmental-insensitive photophysical properties and high quantum yield capable of providing bright blue fluorescence (Fig 10) [48].

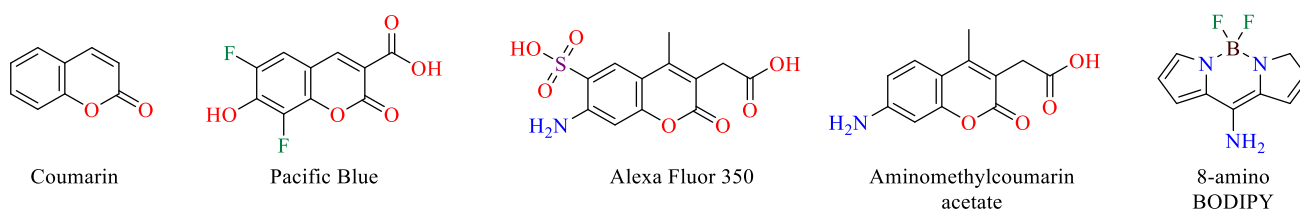


Fig 10. Graphical representation of the blue-emitting fluorophores which are potential candidates for selection in the design of the fluorescence assay.

Protocol A: Qualitative fluorescence assay (Fig 11)

Aim: To determine the penetration and stability of fluorophore within grains and intragrain environmental effects on fluorescence emission.

Procedures:

1. Under aseptic conditions, extract *Madurella mycetomatis* eumycetoma lesions from deep tissue biopsies instead of open sinuses to avoid contamination with other surface pathogens [17].

2. Isolate grains from surrounding granuloma and wash them thoroughly to remove biological debris [17].
3. Separate grains into the experimental group for incubation with fluorophore solution and the control group to account for background fluorescence [49].
4. Measure fluorescence intensity of fluorophore solution using fluorometer with excitation filter of 399 nm and emission filter of 437 nm, corresponding to the peak excitation (λ_{ex}) and emission (λ_{em}) wavelengths for optimal fluorescence [48, 50].
5. To identify optimal fluorophore concentration and incubation period, incubate grains of the experimental group with 8-amino BODIPY solution at various concentrations (e.g. 10 μ M, 20 μ M) in a Petri dish for various incubation periods (e.g. 30 min, 60 min, 90 min), protected from light to prevent photobleaching [47].
6. Following incubation, remove grains and measure the fluorescence intensity of fluorophore solution using a fluorometer⁸ to determine the uptake and leaching potential of fluorophore [50].
7. Thoroughly wash grains to remove excess fluorophore and reduce background fluorescence [49].
8. Perform a qualitative assessment of grain fluorescence using a fluorescence microscope⁸ to examine for fluorophore adsorption to grain exterior surface [50].
9. In preparation for intragrain fluorescence imaging, crush each grain by placing it between two glass slides [51].
10. Prior to mounting coverslip, add antifade mounting reagent to the crushed grain to minimise photobleaching and to protect the fluorescence signal [49].
11. Using a fluorescence microscope⁸, observe for blue intragrain fluorescence indicative of fluorophore penetration and acquire fluorescent photomicrographs [50].
12. Stain crushed grains with Grocott's methenamine silver to highlight fungi location and perform digital microscopy imaging [17].
13. Overlay acquired images with fluorescent photomicrographs to map fluorophore localisation to intragrain components.

⁸ Fluorometer or fluorescence microscope should be fitted with optimal filter set of $\lambda_{ex/em}$: 399 nm/437 nm.

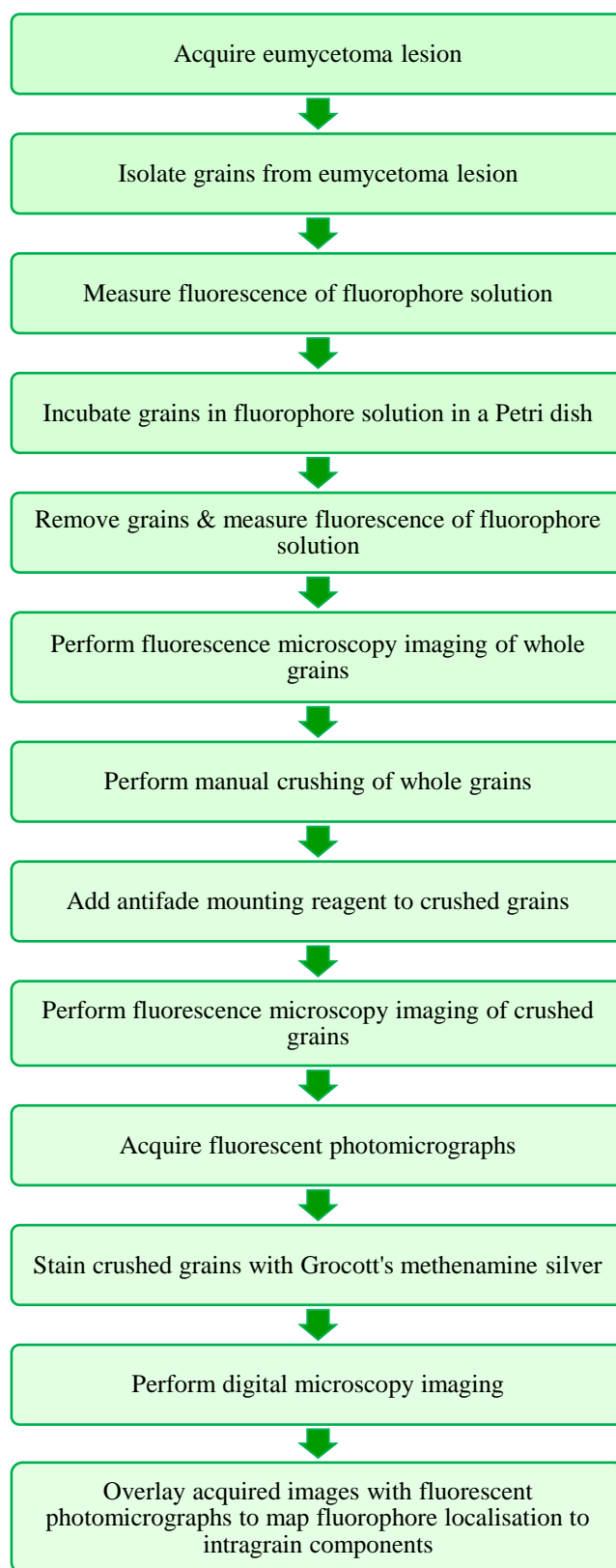


Fig 11. Flowchart of the key procedures in Protocol A: Qualitative fluorescence assay.

Protocol B: Quantitative fluorescence assay ([Fig 12](#))

Aim: After Protocol A is performed, if blue intragrain fluorescence was observed, a quantitative assessment of fluorescence intensity could be conducted to determine the concentration of fluorophore accumulated within the grains.

Procedures:

1. Repeat Steps 1 to 3 of [Protocol A](#).
2. Add a fixed volume of fluorophore solution at previously identified optimal concentration into each well of a microplate and load into a multiplate reader⁹ for measurement of fluorescence intensity [50].
3. Place each acquired grain into a microplate well for incubation with fluorophore solution.
4. Following incubation, remove grains and measure the fluorescence intensity of fluorophore solution using a microplate reader⁹ to determine the uptake and leaching potential of fluorophore [50].
5. Thoroughly wash and resuspend grains in a new microplate [49].
6. Since manual crushing of individual grains is labour-intensive and time-consuming, a plausible alternative would be to place the microplate into a sonication¹⁰ device for automated simultaneous grain disruption.
7. To identify intragrain fluorophore localisation, perform centrifugation to separate grain matrix components from embedded fungi.
8. Transfer supernatant to a new microplate and resuspend fungi pellets.
9. Using a microplate reader⁹, measure fluorescence intensity of supernatant and fungi pellets to determine the accumulation of fluorophore within grain matrix and penetration or adsorption of fluorophore to fungi [48].
10. Average fluorescence intensity of the experimental group following the subtraction of any background fluorescence from the control group could be obtained to determine the concentration of fluorophore accumulated.

⁹ Microplate reader should be fitted with optimal filter set of $\lambda_{\text{ex/em}}$: 399 nm/437 nm.

¹⁰ Sonication could be performed in 30-seconds blocks until visual observation of grain disruption [52].

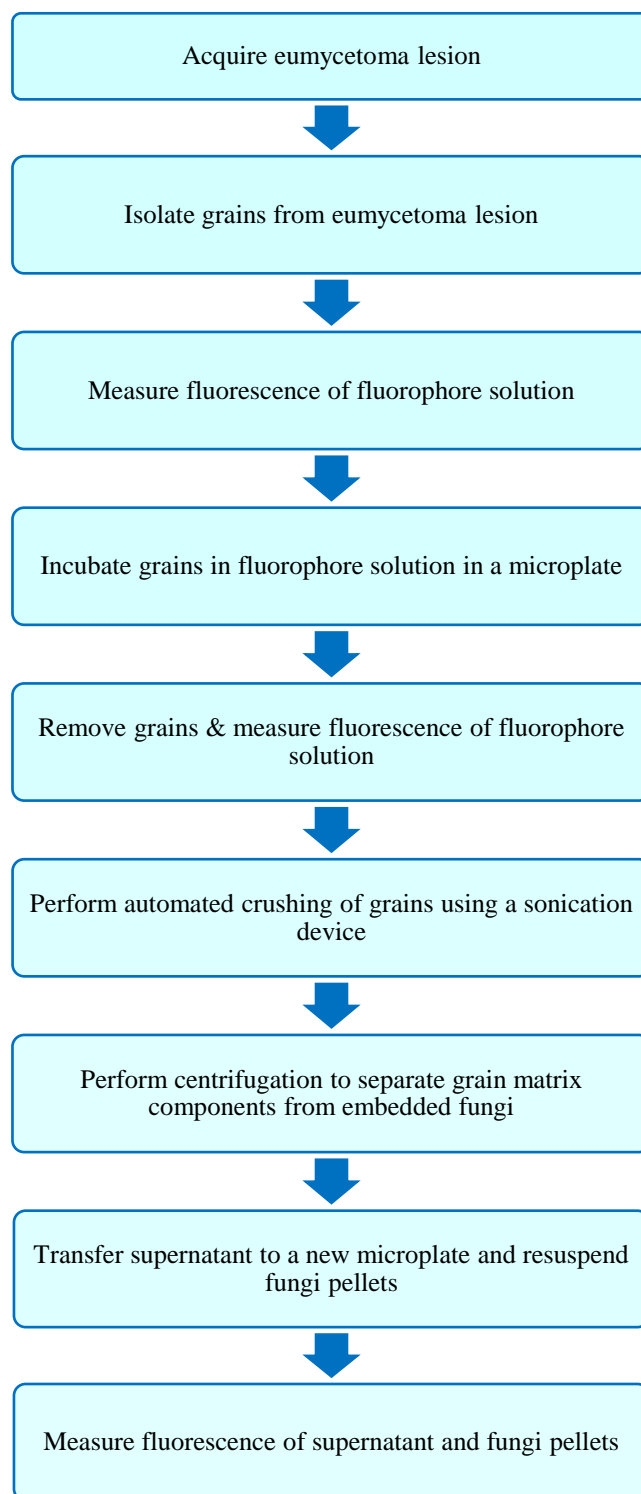


Fig 12. Flowchart of the key procedures in Protocol B: Quantitative fluorescence assay.

As the proposed protocols have not been experimented, the following variables would need to be determined empirically for methodological optimisation through future research:

- Compatibility of selected fluorophore with wash buffer, antifade reagent and grain sample.
- Concentration of fluorophore solution and incubation period.
- Sonication amplitude and timing.
- Centrifugation force and timing.

Conclusion

This study investigated the morphology and composition of *Madurella mycetomatis* grains and the effects of physiochemical properties of compounds on grain penetration. Through the compilation of data on clinically used antifungals and recent screening hits, this enabled a more comprehensive study to be conducted on the under-addressed issue of grain penetration.

In light of the findings of grain structure, grain penetration ability and melanin binding capacity are the key factors which should be considered in the identification and optimisation of future drug candidates. From the data on screening hits and clinically used antifungals, the following were identified:-

- Low lipophilicity is a key determinant in accessing grain-embedded fungi. Hence, four compounds with LogD of ≤ 2.0 at pH 7.4, likely to possess high *in vivo* efficacy were proposed for synthesis to be prioritised.
- Structural moieties facilitating fungal melanin binding interaction such as dichlorobenzene ring, extended polyaromatic side chain and positively-charged structures should be avoided in the design of future drug candidates for their accessibility to drug targets.
- The molecular size of compounds as defined by their molecular weight and volume was not identified as a dominating determinant of *in vivo* efficacy.

This study additionally proposed protocols for a first-ever fluorescence assay to determine *M. mycetomatis* grain penetration by small molecules, whose feasibility could be investigated in future work.

Supporting Information

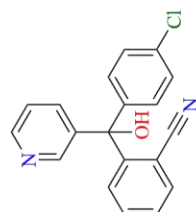
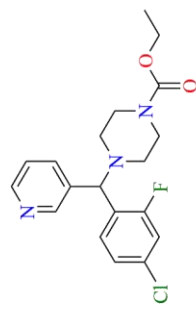
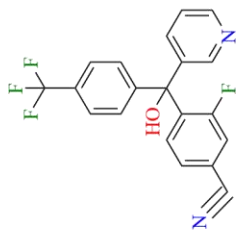
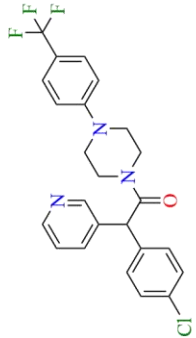
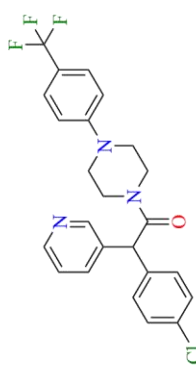
S1 Appendix. Eumycetoma antifungal compounds.

S2 Appendix. *Madurella mycetomatis* eumycetoma grain model.

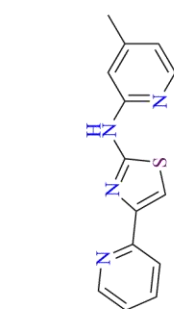
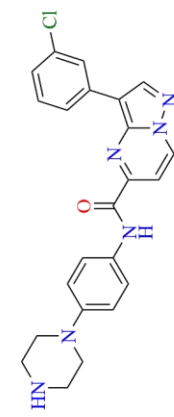
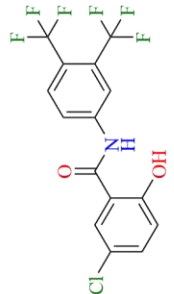
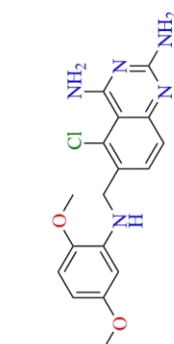
S3 Appendix. Additional statistical test results.

S1 Appendix: Eumycetoma antifungal compounds

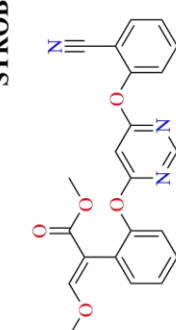
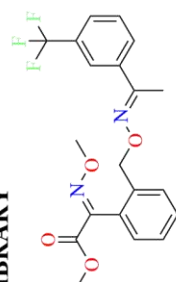
FENARIMOL ANALOGUES FROM ORIGINAL LIBRARY

				
EPL-BS0178 1.25, 1.8, 8 2.3 320.78 277.62	EPL-BS0495 0.28, 0.46, 4 2.5 377.84 329.86	EPL-BS0800 0.58, 0.87, 4 3.1 372.32 300.31	EPL-BS1246 (S) 1.53, 2.89, 4 3.5 459.90 385.28	EPL-BS1025 (rac) 0.63, 0.94, 4 3.5 459.90 385.28

OTHER COMPOUNDS FROM ORIGINAL LIBRARY

			
MMV006357 0.40, 1.10, 0.25 2.2 268.34 234.07	MMV022478 2.95, 4.90, 4 3.1 432.91 374.38	MMV687807 1.45, 3.80, 2 4.6 383.67 270.99	MMV675968 2.30, 4.70, 2 2.0 359.81 307.54

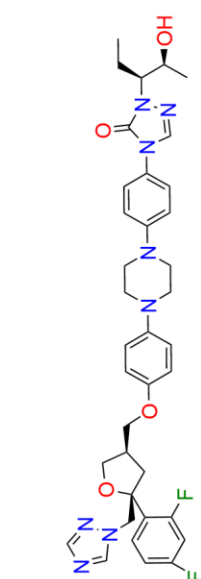
STROBILURINS FROM ORIGINAL LIBRARY

	
MMV021057 (Azoxystrobin) 0.6, 20.45, 0.06 4.0 403.39 350.87	MMV68754 (Trifloxystrobin) 1.05, 28.10, 0.25 4.2 403.38 345.69

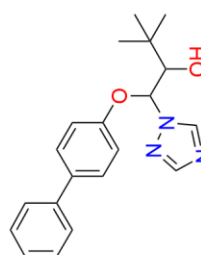
Compound code
IC ₅₀ (mM), IC ₉₀ (mM), MIC ₅₀ (mM)
LogD at pH7.4
Molecular weight (Da)
Molecular volume (Å ³)

S1 Appendix-continued

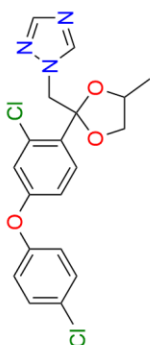
AZOLES FROM ORIGINAL LIBRARY



MMV688774 (Posaconazole)
 $<0.1, <0.1, <0.004$
 3.5
 700.79
 623.35

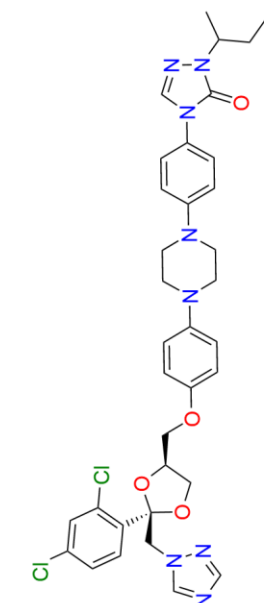


MMV68942 (Biteranol)
 $<0.1, <0.1, 0.06$
 4.2
 337.42
 320.76

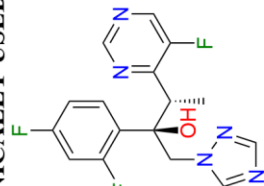


MMV688943 (Difenconazole)
 $<0.1, <0.1, 0.06$
 4.3
 406.26
 330.60

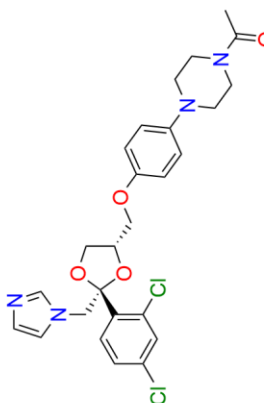
CLINICALLY USED AZOLES



Itraconazole
 0.06
 4.5
 705.64
 607.90

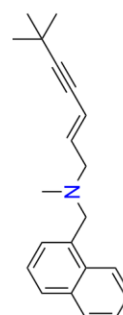


Voriconazole
 0.125
 2.5
 349.32
 285.11

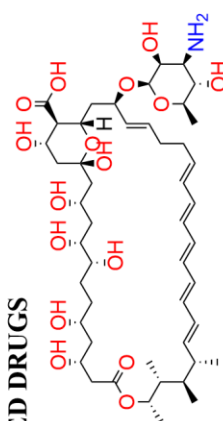


Ketoconazole
 0.125
 3.0
 531.43
 452.47

OTHER CLINICALLY USED DRUGS



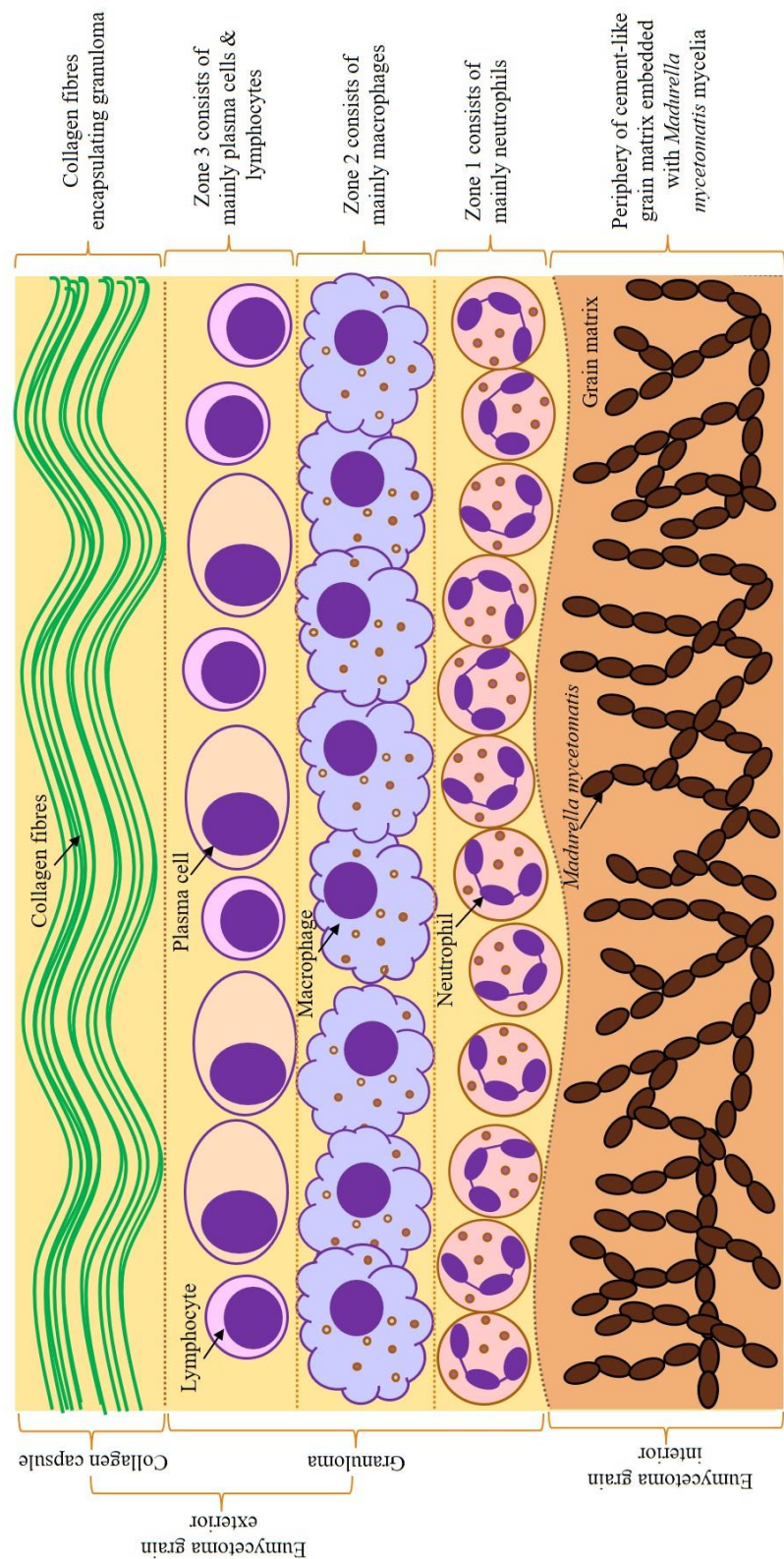
Terbinafine
 8
 3.6
 291.44
 306.73



Amphotericin B
 2
 1.1
 924.14
 865.48

Compound code
 IC₅₀ (mM), IC₉₀ (mM), MIC₅₀ (mM)
 LogD at pH7.4
 Molecular weight (Da)
 Molecular volume (Å³)

S2 Appendix: *Madurella mycetomatis* eumycetoma grain model



S3 Appendix: Additional statistical test results

Shapiro-Wilk test results

	Table 1 compounds		Table 2 compounds	
	LogD at pH 7.4 values	Percentage larval survival values	LogD at pH 7.4 values	Percentage larval survival values
<i>p</i> values	0.402	0.727	0.174	0.776
Degree of freedom	14		6	
α	0.05			
H ₀ , Null hypothesis	Data is normally distributed. H ₀ accepted if <i>p</i> >0.05.			
H ₁ , Alternative hypothesis	Data is not normally distributed. H ₁ accepted if <i>p</i> <0.05.			
Conclusion	The calculated <i>p</i> values are greater than α of 0.05, hence, the null hypothesis that both data variables are normally distributed were accepted.			

Interpretation of Pearson's product-moment correlation coefficient

Pearson's product-moment correlation coefficient was interpreted using a conventional stratification listed below [38].	
Magnitude of correlation coefficient	Interpretation of correlation
0.00-0.09	Negligible
0.10-0.39	Weak
0.40-0.69	Moderate
0.70-0.89	Strong
0.90-1.00	Very strong

Acknowledgements

The authors of this study gratefully acknowledge Professor Matthew Todd for the guidance provided throughout the research project. This research would not have been possible without the provision of input from Dr. Wendy van de Sande of Erasmus Medical Centre and data from Dr. Benjamin Perry of DNDi.

References

1. Zijlstra EE, van de Sande WWJ, Welsh O, Mahgoub ES, Goodfellow M, Fahal AH. Mycetoma: a unique neglected tropical disease. *The Lancet Infectious Diseases*. 2016;16(1):100-12.
2. de Hoog GS, Ahmed SA, Najafzadeh MJ, Sutton DA, Keisari MS, Fahal AH, et al. Phylogenetic Findings Suggest Possible New Habitat and Routes of Infection of Human Eumycetoma (Possible Mycetoma Habitat). *Plos Neglect Trop Dis*. 2013;7(5):e2229.
3. van de Sande WWJ. Global Burden of Human Mycetoma: A Systematic Review and Meta-analysis. *Plos Neglect Trop Dis*. 2013;7(11):e2550.
4. Nenoff P, van de Sande WWJ, Fahal AH, Reinell D, Schofer H. Eumycetoma and actinomycetoma - an update on causative agents, epidemiology, pathogenesis, diagnostics and therapy. *J Eur Acad Dermatol Venereol*. 2015;29(10):1873-83.
5. van de Sande WWJ, Fahal AH, Ahmed SA, Serrano JA, Bonifaz A, Zijlstra E, et al. Closing the mycetoma knowledge gap. *Medical Mycology*. 2018;56:S153-S64.
6. (DNDi) DfNDi. Mycetoma: New hope for neglected patients? DNDi. Online: DNDi; 2019. p. 1-12.
7. Findlay GH, Vismer HF. Black grain mycetoma: A Study Of The Chemistry, Formation And Significance Of The Tissue Grain In *Madurella* Mycetomi Infection. *British Journal of Dermatology*. 1974;91(3):297-303.
8. van de Sande WWJ, van Vianen W, ten Kate M, Fahal AH, Bakker-Woudenberg I. Amphotericin B but not itraconazole is able to prevent grain formation in experimental *Madurella mycetomatis* mycetoma in mice. *British Journal of Dermatology*. 2015;173(6):1561-2.
9. Kloezen W, van Helvert-van Poppel M, Fahal AH, van de Sande WWJ. A *Madurella mycetomatis* Grain Model in *Galleria mellonella* Larvae. *Plos Neglect Trop Dis*. 2015;9(7):e0003926.
10. Perdoni F, Falleni M, Tosi D, Cirasola D, Romagnoli S, Braidotti P, et al. A histological procedure to study fungal infection in the wax moth *Galleria mellonella*. *Eur J Histochem*. 2014;58(3):258-62.
11. Kloezen W, Parel F, Brüggemann R, Asouit K, Helvert-van Poppel M, Fahal A, et al. Amphotericin B and terbinafine but not the azoles prolong survival in *Galleria mellonella* larvae infected with *Madurella mycetomatis*. *Medical mycology*. 2018;56(4):469.
12. van de Sande WWJ, de Kat J, Coppens J, Ahmed AOA, Fahal A, Verbrugh H, et al. Melanin biosynthesis in *Madurella mycetomatis* and its effect on susceptibility to itraconazole and ketoconazole. *Microbes and Infection*. 2007;9(9):1114-23.
13. Nyuykonge B, Croughs PD, Fahal AH, Verbon AH, van de Sande WWJ. Pyomelanin Secretion in Interferes with Spectrophotometrically End-point Reading using the Sensititre™ YeastOne™ Alamar Blue Assay but not with Visual End-point Reading. *Antimicrob Agents Chemother*. 2019.
14. Eadie K, Parel F, Helvert-van Poppel M, Fahal AH, van de Sande WWJ. Combining two antifungal agents does not enhance survival of *Galleria mellonella* larvae infected with *Madurella mycetomatis*. *Trop Med Int Health*. 2017;22(6):696-702.

15. Lim W, Melse Y, Konings M, Hung PD, Eadie K, Laleu B, et al. Addressing the most neglected diseases through an open research model: The discovery of fenarimols as novel drug candidates for eumycetoma. *Plos Neglect Trop Dis*. 2018;12(4):e6437.
16. Open Source Drug Discovery for Mycetoma Online: GitHub Inc.; 2019 [updated 2019; cited 2019. New Medicines for Mycetoma without Secrecy]. Available from: <https://github.com/OpenSourceMycetoma>.
17. Ahmed AA, van de Sande WWJ, Fahal AH. Mycetoma laboratory diagnosis: Review article. *Plos Neglected Tropical Diseases*. 2017;11(8):17.
18. Geneugelijck K, Kloezen W, Fahal AH, van de Sande WWJ. Active Matrix Metalloprotease-9 Is Associated with the Collagen Capsule Surrounding the *Madurella mycetomatis* Grain in Mycetoma. *Plos Neglect Trop Dis*. 2014;8(3):e2754.
19. Mhmoud NA, Yousif B, Fahal AH, van de Sande WWJ. Characterisation of the *Madurella mycetomatis* mycetoma granuloma tissue pigments and fibrous tissue. *Khartoum Medical Journal*. 2016;8:1104-10.
20. Emmanuel Edwar S, Ali Mahmoud Mohammed E, Sahar Mubarak B, Wendy WJvdS, Ahmed Hassan F. Interleukin-17 and matrix metalloprotease-9 expression in the mycetoma granuloma. *PLoS Neglected Tropical Diseases*. 2019;13(7):e0007351.
21. Mhmoud NA, Fahal AH, van de Sande WWJ. The association between the interleukin-10 cytokine and CC chemokine ligand 5 polymorphisms and mycetoma granuloma formation. *Medical Mycology*. 2013;51(5):527-33.
22. Relhan V, Mahajan K, Agarwal P, Garg VK. Mycetoma: An Update. *Indian Journal of Dermatology*. 2017;62(4):332.
23. Wethered DB, Markey MA, Hay RJ, Mahgoub ES, Gumaa SA. Ultrastructural and immunogenic changes in the formation of mycetoma grains. *Journal of Medical and Veterinary Mycology*. 1987;25(1):39-46.
24. Verwer PEB, Notenboom CC, Eadie K, Fahal AH, Verbrugh HA, van de Sande WWJ. A Polymorphism in the Chitotriosidase Gene Associated with Risk of Mycetoma Due to *Madurella mycetomatis* Mycetoma—A Retrospective Study (Chitinases in *Madurella mycetomatis* Mycetoma). *Plos Neglect Trop Dis*. 2015;9(9):e0004061.
25. van de Sande WWJ, Fahal AH, Bakker-Woudenberg IAJM, van Belkum A. *Madurella mycetomatis* Is Not Susceptible to the Echinocandin Class of Antifungal Agents. *Antimicrob Agents Chemother*. 2010;54(6):2738.
26. Ibrahim AI, Hassan AME, Fahal AH, van de Sande WWJ. A histopathological exploration of the *Madurella mycetomatis* grain. *PLoS ONE*. 2013;8(3):e57774.
27. Findlay GH, Vismer HF, Botes D, Kruger H. Black grain mycetoma: Studies on the pigment of *Madurella mycetomi*. *Mycopathologia*. 1980;70(1):61-4.
28. Eisenman HC, Nosanchuk JD, Webber JBW, Emerson RJ, Camesano TA, Casadevall A. Microstructure of cell wall-associated melanin in the human pathogenic fungus *Cryptococcus neoformans*. *Biochemistry*. 2005;44(10):3683-93.
29. Nosanchuk JD, Stark RE, Casadevall A. Fungal Melanin: What do We Know About Structure? *Front Microbiol*. 2015;6:7.
30. Cordero RJB, Casadevall A. Functions of fungal melanin beyond virulence. *Fungal Biology Reviews*. 2017;31(2):99-112.
31. Gerwien F, Skrahina V, Kasper L, Hube B, Brunke S. Metals in fungal virulence. *Fems Microbiology Reviews*. 2018;42(1):1-21.
32. Welsh O, Al-Abdely HM, Salinas-Carmona MC, Fahal AH. Mycetoma Medical Therapy. *Plos Neglect Trop Dis*. 2014;8(10):8.
33. Nasher M, Wethered D, Hay RJ, Mahgoub ES, Gumaa SA. The Ultrastructure Of Actinomycetoma Grains Caused By *Streptomyces-Somaliensis*. *Am J Trop Med Hyg*. 1987;37(1):174-9.
34. Hassan AME, Fahal AH, Ahmed AO, Ismail A, Veress B. The immunopathology of actinomycetoma lesions caused by *Streptomyces somaliensis*. *Trans Roy Soc Trop Med Hyg*. 2001;95(1):89-92.
35. Hay RJ. A thorn in the flesh--a study of the pathogenesis of subcutaneous infections. *Clinical and experimental dermatology*. 1989;14(6):407-15.

36. Perry B. StarDrop LogD at pH7.4 values. In: Rosalyn LZ C, editor. Open Source Mycetoma (MycetOS)2019.
37. Vetter TR. Fundamentals of Research Data and Variables: The Devil Is in the Details. *Anesth Analg*. 2017;125(4):1375-80.
38. Schober P, Boer C, Schwarte LA. Correlation Coefficients: Appropriate Use and Interpretation. *Anesth Analg*. 2018;126(5):1763-8.
39. Palm K, Luthman K, Unge A, Strandlund G, Artursson P. Correlation of Drug Absorption with Molecular Surface Properties. *Journal of Pharmaceutical Sciences*. 1996;85(1):32-9.
40. Hou T, Zhang W, Xia K, Qiao W, Xu X. ADME evaluation in drug discovery. 5. Correlation of caco-2 permeation with simple molecular properties. *Journal of Chemical Information and Computer Sciences*. 2004;44(5):1585-600.
41. Perry B. Molecule size & effects on grain penetration Online: Open Source Mycetoma (MycetOS); 2019 [cited 2019 12/12/2019]. Available from: <https://github.com/OpenSourceMycetoma/Series-1-Fenarimols/issues/24#issuecomment-564564485>.
42. Eisenman HC, Casadevall A. Synthesis and assembly of fungal melanin. *Applied Microbiology and Biotechnology*. 2012;93(3):931-40.
43. Nosanchuk JD, Valadon P, Feldmesser M, Casadevall A. Melanization of *Cryptococcus neoformans* in murine infection. *Mol Cell Biol*. 1999;19(1):745-50.
44. Hopkins LA, Bickerton RG. Drug discovery: Know your chemical space. *Nature Chemical Biology*. 2010;6(7):482.
45. van de Sande WWJ. Suggestion for compounds capable of penetrating fungal grains GitHub: Open Source Mycetoma (MycetOS); 2019 [cited 2019 8/11/2019]. Available from: <https://github.com/OpenSourceMycetoma/Series-1-Fenarimols/issues/23#issuecomment-551844807>.
46. Singha S, Kim D, Roy B, Sambasivan S, Moon H, Rao AS, et al. A structural remedy toward bright dipolar fluorophores in aqueous media. *Chemical Science*. 2015;6(7):4335-42.
47. Kim D, Ma D, Kim M, Jung Y, Kim NH, Lee C, et al. Fluorescent Labeling of Protein Using Blue-Emitting 8-Amino-BODIPY Derivatives. *Journal of Fluorescence*. 2017;27(6):2231-8.
48. Banuelos J, Martin V, Gomez-Duran CFA, Cordoba IJA, Pena-Cabrera E, Garcia-Moreno I, et al. New 8-Amino-BODIPY Derivatives: Surpassing Laser Dyes at Blue-Edge Wavelengths. *Chemistry*. 2011;17(26):7261-70.
49. Invitrogen. The Molecular Probes Handbook—A Guide to Fluorescent Probes and Labeling Technologies. Online: Thermo Fisher Scientific Inc.; 2010 [cited 2019 24/11/2019]. Available from: <https://www.thermofisher.com/uk/en/home/life-science/cell-analysis/cell-analysis-learning-center/molecular-probes-school-of-fluorescence.html>.
50. Kim NH, Kim D. Blue-Emitting BODIPY Dyes. BODIPY Dyes - A Privilege Molecular Scaffold with Tunable Properties. Online: InTechOpen; 2018.
51. van de Sande WWJ. Project Launch. 2. Which Fenarimol Analogs Should be Made Next? 10/12/2019 ed. GitHub Open Source Mycetoma (MycetOS): Open Source Mycetoma (MycetOS); 2018.
52. Scientific TF. Imaging Basics Online: Thermo Fisher Scientific Inc.; 2019 [cited 2019 25/11/2019]. Available from: <https://www.thermofisher.com/uk/en/home/life-science/cell-analysis/cell-analysis-learning-center/molecular-probes-school-of-fluorescence/imaging-basics/capturing-analyzing-your-samples/exposure-times.html>.